Journal of Power Sources 195 (2010) 2557–2563

Contents lists available at ScienceDirect

Journal of Power Sources

journal homepage: www.elsevier.com/locate/jpowsour

Highly stable platinum electrocatalysts for oxygen reduction formed using supercritical fluid impregnation

Shee-Yen Ang, Darren A. Walsh*

School of Chemistry and Faculty of Engineering, The University of Nottingham, Nottingham NG7 2RD, UK

ARTICLE INFO

Article history:
Received 16 July 2009
Received in revised form
30 September 2009
Accepted 21 October 2009
Available online 13 November 2009

Keywords:
Fuel cell
Electrocatalysis
Supercritical carbon dioxide
Rotating-disk electrode
Oxygen reduction

ABSTRACT

A carbon-supported platinum electrocatalyst for the oxygen reduction reaction (ORR) in acidic medium was synthesised using supercritical fluid impregnation. The catalytic performance and electrochemical stability of this catalyst were studied using voltammetric and microscopic analysis. The results from these analyses were compared with those obtained using a Pt/C catalyst formed using a traditional wet chemical method (reduction of H_2PtCl_6 in aqueous solution using $NaBH_4$). In the supercritical impregnation method, carbon black (Vulcan XC72R) was impregnated with (1,5-cyclooctadiene)dimethyl platinum(II), $PtMe_2COD$, in supercritical carbon dioxide ($scCO_2$) at 1200 p.s.i and 40 °C. After depressurisation, carbon-supported Pt nanoparticles were formed by thermally decomposing the adsorbed $PtMe_2COD$. An accelerated stability test was performed, which revealed morphological changes in the electrocatalysts, which were significantly more pronounced in the Pt/C formed using the wet chemical method. Electrochemical analysis also showed that the Pt/C formed using wet chemistry lost a significant proportion of its electrochemical surface area after potential cycling, whereas that formed using $scCO_2$ did not. Furthermore, the Pt/C formed in $scCO_2$ retained its electrocatalytic activity to a significantly larger extent. The stability of the electrocatalysts formed using $scCO_2$ processing suggests that this approach may be promising for the fabrication of more stable fuel cell cathodes than are currently available.

1. Introduction

The widespread use of fuel cell technology as a replacement for current energy conversion devices depends on the development of low-cost, efficient fuel cells. In proton exchange membrane fuel cells (PEMFCs), platinum-based catalysts are used for hydrogen oxidation and oxygen reduction. However, sluggish reaction kinetics, particularly of the oxygen reduction reaction (ORR) at platinum, is one of the factors limiting the efficiency and commercial viability of PEMFCs. Therefore, the development of more efficient, less expensive fuel cell electrodes is currently the goal of many research efforts. This includes the development of platinum alloys, which can increase efficiency and reduce the required platinum loading [1–3], and the use of novel support materials that can increase electrocatalyst utilisation and efficiency [4,5]. Several groups have also reported non-platinum metal alloys that compete with platinum in terms of electrocatalytic activity for the ORR [6–8]. A common goal in all fuel cell electrocatalyst syntheses is to fabricate well dispersed metal nanoparticles with a small particle size distribution. Chemical reduction of platinum salts [9,10], physical sputtering [11], plasma reduction [12] and polyol processes [13,14] have all been used with varying degrees of success.

Durability is also a major issue in fuel cell research and development and the U.S. Department of Energy has listed lifetime targets, which include a 2010/2015 target of 5000 h for PEMFCs in transportation applications and a 2011 target of 40,000 h for integrated stationary PEMFCs [15]. In operational fuel cells, platinum dissolution and redeposition can cause particle growth and the formation of Pt deposits within the electrolyte membrane [16,17]. In addition, electrocatalyst particle migration and coalescence can occur [18]. These can lead to rapid loss of Pt surface area and a drop in power output. This is more problematic when the power demands are altered continuously, such as in the stop–start operation of automobiles, than when the cell is operated at constant voltage [19,20]. A number of methods for stabilising Pt-based ORR electrocatalysts against loss of surface area have appeared in the literature recently, which include the use of bimetallic Pt/Pd nanodendrites [21] and Pt nanoparticles decorated with Au clusters [22] as catalysts, and the use of novel nitrogen-modified carbon composites as the catalyst support [23].

The synthesis of nanomaterials using supercritical fluids as "green" solvents has become increasingly popular in recent years [24–26]. Supercritical carbon dioxide ($scCO_2$) is particularly attractive for materials processing as it is accessible under moderate conditions (T_c = 31 °C and P_c = 7.38 MPa), abundant, inexpensive,

* Corresponding author. Tel.: +44 115 9513437; fax: +44 115 9513562.
E-mail address: darren.walsh@nottingham.ac.uk (D.A. Walsh).

0378-7753/$ – see front matter © 2009 Elsevier B.V. All rights reserved.
doi:10.1016/j.jpowsour.2009.10.097

non-flammable, non-toxic, and environmentally benign [27–29]. In recent years, these advantages have been exploited by a number of groups for the development of fuel cell electrodes. For example, Lin et al. recently synthesised platinum/carbon nanotube nanocomposites for methanol oxidation using $scCO_2$ [30]. Erkey and co-workers have also synthesised nanocomposite electrocatalysts for fuel cells using $scCO_2$ as the processing medium [31–33]. Bimetallic platinum-based electrocatalyst nanoparticles supported on carbon nanotubes for direct methanol fuel cells have also been produced using $scCO_2$ [34,35].

In this contribution, we describe the synthesis and electrochemical stability of a Pt/C ORR electrocatalyst synthesised using $scCO_2$ as the processing medium and compare its activity and stability with that of a Pt/C electrocatalyst formed using a standard wet chemical method. In the $scCO_2$ synthesis, the precursor was (1,5-cyclooctadiene)dimethyl platinum(II), $PtMe_2COD$, which was adsorbed on carbon black (Vulcan XC72R). After depressuring the CO_2, carbon-supported platinum nanoparticles were formed by thermal decomposition of the precursor in an inert atmosphere. The wet chemical method used for comparison was reduction of H_2PtCl_6 using sodium borohydride in aqueous solution in the presence of Vulcan XC72R. The morphology of each Pt/C sample was characterised using powder X-ray diffraction (XRD) and transmission electron microscopy (TEM). The electrocatalytic activity of each electrocatalyst for the ORR was determined before and after an accelerated stability test, in which the catalysts were subjected to repeated potential cycling in 0.5 M H_2SO_4. The electrocatalytic stability of each electrocatalyst was then correlated with morphological changes observed after electrochemical cycling. The results described here demonstrate that, not only is supercritical fluid processing a very clean alternative to traditional methods for electrocatalyst development, it may offer enhancements in terms of electrocatalyst lifetime and durability.

2. Experimental

2.1. Materials and apparatus

All reagents were purchased from Sigma–Aldrich and were used as received. Carbon black (Vulcan XC72R) was obtained from Cabot Co. (Boston, MA). Electrochemical measurements were performed using a Model CHI760C potentiostat from CH Instruments (Austin, TX), a glassy carbon rotating-disk electrode assembly and Model MSR Modulated Speed Rotator from Pine Instruments (Raleigh, NC).

2.2. Wet chemical synthesis of Pt/C electrocatalysts

Hexachloroplatinic acid (32.8 mg) was dissolved in 50 mL deionised water in the presence of 35.7 mg Vulcan XC72R and sonicated for several minutes to achieve a well dispersed suspension. 0.5 M NaOH was then added dropwise under stirring until the pH was approximately 10. $NaBH_4$ (0.02 M) was then added at 10 times molar excess of H_2PtCl_6 while sonicating. The reaction was left overnight to ensure complete reduction of the H_2PtCl_6. The resulting Pt/C was then filtered, washed with copious amounts of deionised water, and dried at 60 °C. The total metal loading, as determined using thermogravimetric analysis (TGA), was 30%. In the text, we refer to this catalyst as Pt/C(H_2O).

2.3. Synthesis of Pt/C using $scCO_2$

Pt/C was prepared in $scCO_2$ using a procedure similar to that reported by Erkey and co-workers [33]. Prior to use, a home-built 60 mL stainless steel autoclave was flushed with CO_2 for several minutes. 120 mg of Vulcan XC72R and $PtMe_2COD$ were then added to the autoclave and CO_2 was then injected via a Pickel pump (NWA Analytics) to a pressure of 1200 psi. $PtMe_2COD$ was added at a concentration of 6.67 mg g^{-1} CO_2, giving a targeted total metal loading of 30 wt% (described in Section 3.1). The temperature of the autoclave was raised to 40 °C using an electrically heated jacket surrounding the autoclave. The mixture was then allowed to stir overnight to ensure that the precursors fully diffused into the substrate. The CO_2 was then slowly released and the impregnated Vulcan XC72R was recovered from the autoclave. The adsorbed precursors were converted to elemental platinum by thermal decomposition in a tube furnace under flowing nitrogen (at atmospheric pressure) for 3 h at 300 °C. Subsequently, the furnace was turned off and the Pt/C was allowed to cool to room temperature under flowing N_2. In the text we refer to this catalyst as Pt/C($scCO_2$).

2.4. Morphological and electrochemical charaterisation of Pt/C electrocatalysts

Catalyst suspensions were prepared for TEM analysis by dispersing the Pt/C composites in acetone. Carbon TEM grids were coated with the suspension and allowed to dry in air before imaging using a JEOL 2100F TEM, operated at 200 kV. Powder XRD was performed by bombarding the sample with an X-ray beam from a copper K_α source ($\lambda = 0.154$ nm) and recording reflections from 10° to 80° at 0.04° increments in diffraction mode. For electrochemical analysis, a 5 mm diameter glassy carbon (GC) disk electrode was used. An Ag|AgCl reference electrode and platinum wire counter electrode completed the electrochemical cell. However, all potentials are reported versus the standard hydrogen electrode (SHE). Prior to use, the electrode was polished using aqueous alumina suspensions with successively smaller particle sizes between 1 μm and 0.05 μm on felt polishing pads. Catalyst inks were prepared by dispersing the Pt/C electrocatalysts in 80:20 water/ethanol to a loading of 2 mg mL^{-1}. Nafion (5 wt% in ethanol) was diluted 1:80 with water and the resulting solution was mixed with an equal volume of the catalyst ink. 30 μL of the resulting suspension was drop cast onto the GC surface and the assembly was dried for 20 min at 60 °C. Rotating-disk electrode experiments were performed by rotating the electrode (rotation rates are described in Section 3.3) and sweeping the potential of the GC disk in a negative potential direction (initial and final potentials are described in Section 3.3) at 5 mV s^{-1} and recording the current for oxygen reduction.

3. Results and discussion

3.1. Supercritical fluid impregnation and reduction of $PtMe_2COD$

The uptake of the $PtMe_2COD$ by the carbon within $scCO_2$ is governed by the thermodynamics and kinetics of adsorption and the adsorption isotherm for $PtMe_2COD$ uptake by functionalised multiwalled carbon nanotubes (MWCNTs) in $scCO_2$ was recently published [36]. Based on this work, we chose a concentration of 6.67 mg $PtMe_2COD$ per g $scCO_2$ to target a metal loading of 20 wt% with the assumption of similar adsorption behaviour on the Vulcan XC72R. After adsorption, it is possible to reduce the precursors to metal using a number of approaches and we chose thermal decomposition as this can promote smaller average metal particle sizes [37]. The thermal decomposition temperature of $PtMe_2COD$ is approximately 175 °C, at which temperature it decomposes into volatile hydrocarbon and elemental platinum [31]. Therefore, a relatively high temperature of 300 °C was chosen for the reaction to ensure complete decomposition of $PtMe_2COD$ and volatilisation of the ligands from the carbon. Using these conditions, the average total metal loading of the Pt/C($scCO_2$), determined using TGA, was 24 ± 4 wt%, suggesting that the thermodynamics of adsorption at

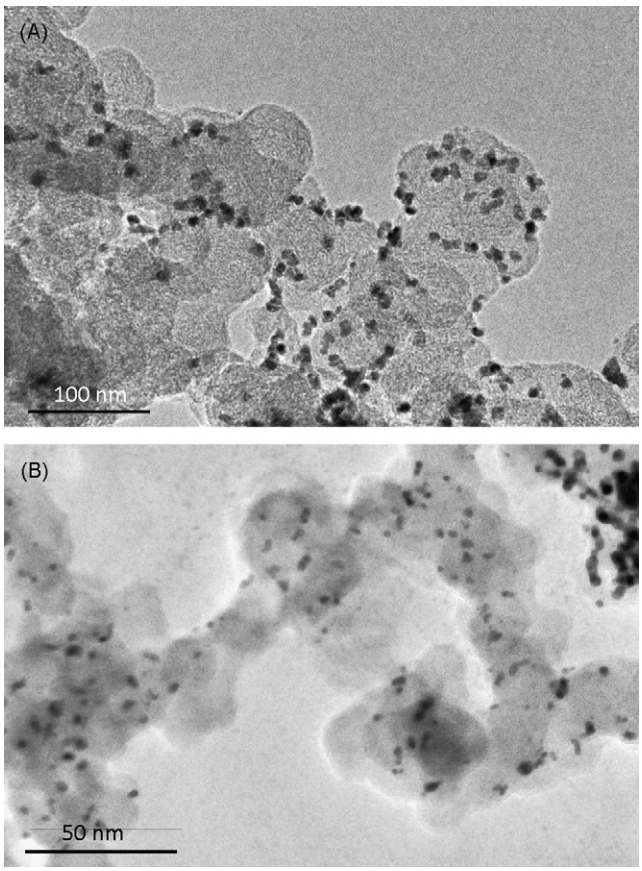

Fig. 1. TEM images of Pt/C samples prepared using (A) wet chemical reduction of H_2PtCl_6 and (B) $scCO_2$ impregnation of Vulcan XC72R with $PtMe_2COD$ and thermal reduction.

Vulcan XC72R are similar to those observed at MWCNTs and that complete reduction of adsorbed $PtMe_2COD$ to Pt occurred.

3.2. Morphological analysis of Pt/C electrocatalysts

In the development of novel electrocatalysts for fuel cells, the electrocatalyst performance usually depends on several factors including the dispersion of the electrocatalyst nanoparticles on the carbon support, the average platinum particle size, and the crystallite geometry. Transmission electron microscopy (TEM) was used to examine the morphology of the electrocatalysts prepared using each method and Fig. 1 shows typical TEM images obtained for each sample. In each sample, Pt nanoparticles with average diameters in the range 1–5 nm were observed. However, the Pt nanoparticles in the Pt/C($scCO_2$) sample appeared to be slightly more uniformly dispersed on the carbon support than those in Pt/C(H_2O). Fig. 2 shows the particle size distribution determined for each Pt/C sample. The average Pt nanoparticle diameters, estimated from TEM analysis, were 4.2 nm and 3.7 nm for Pt/C(H_2O) and Pt/C($scCO_2$), respectively. It is generally agreed that the optimum Pt nanoparticle size for ORR electrocatalysis lies in the range 1–5 nm [38–43] and Fig. 2 shows that each method yielded nanoparticles with average sizes that lie within this range.

Powder X-ray diffraction was used to examine the composition and morphology of the particles formed using each method and Fig. 3 shows typical diffractograms recorded at each Pt/C sample. The peak at $2\theta = 25^\circ$ is due to the Vulcan XC72R support, while three reflections were visible in each sample, corresponding to the (1 1 1), (2 0 0) and (2 2 0) planes of the pure platinum fcc phase [44]. The volume average crystallite size in each catalyst sample can be

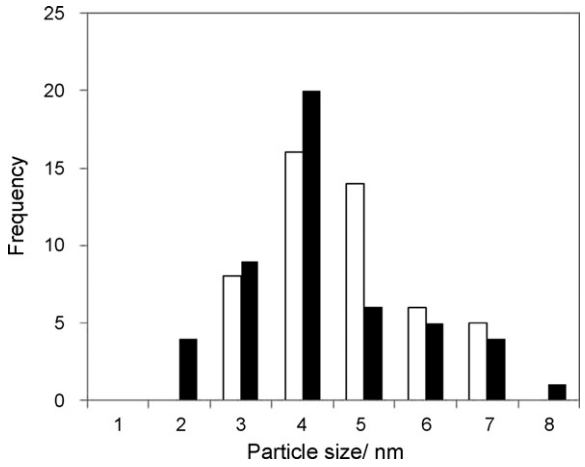

Fig. 2. Particle size distribution of the Pt/C samples prepared using each method. The black columns show the distribution for the Pt nanoparticles formed in $scCO_2$ and the colourless columns show the distribution for the Pt nanoparticles formed using wet chemical reduction of H_2PtCl_6. In each case, 50 particles were measured.

estimated from the diffractogram in conjunction with the Scherrer formula ($d = 0.9\lambda/\beta\cos\theta$, where β is the full width at half maximum peak height measured at the diffraction angle θ). By fitting the peak due to the (1 1 1) reflection at $2\theta = 40^\circ$ to a Gaussian curve, the average crystallite sizes were 4.8 nm and 7.9 nm for the Pt/C($scCO_2$) and Pt/C(H_2O), respectively. These values are slightly higher than the number-averaged particle diameters determined using TEM and may be due to the fact that the Scherrer formula yields a volume-based average size, to which the largest particles can contribute disproportionately [45,46]. Therefore, as the TEM analysis is based on a statistical analysis of particles in the images, we assume here that the TEM analysis yielded more reliable average Pt particle sizes.

3.3. Electrochemical characterisation of Pt/C electrocatalysts

Fig. 4 shows typical cyclic voltammograms (CVs) obtained at Pt/C-modified GC electrodes in deoxygenated 0.5 M H_2SO_4. Each CV is similar to that observed at polycrystalline Pt electrodes [47], showing peaks for the adsorption and desorption of hydrogen between 0.0 and 0.3 V. Oxidation of the platinum surface began at about 0.9 V in the forward sweep in each case and reduction of the platinum oxide occurred on the reverse sweep. The electrochemical surface area (ESA) can be estimated by integrating the charge

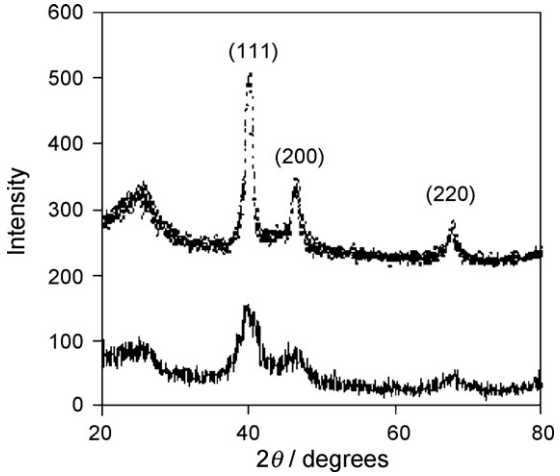

Fig. 3. X-ray diffractogram of the Pt/C samples synthesised using $scCO_2$ (solid line) and aqueous deposition (dashed line).

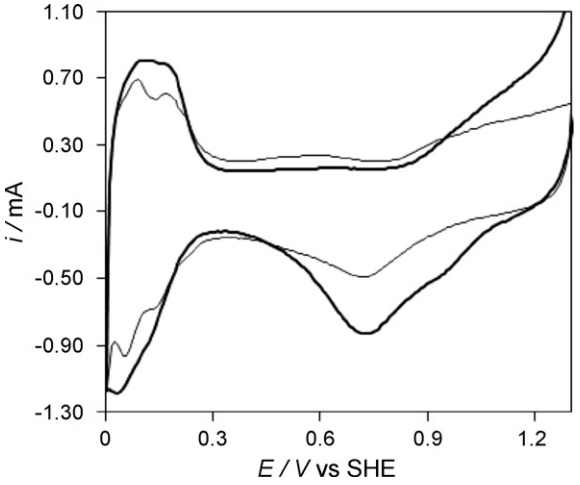

Fig. 4. Cyclic voltammograms of Pt/C electrocatalysts in deoxygenated 0.5 M H_2SO_4 at 25 °C at a scan rate of 0.5 V s^{-1} from 0.0 V to 1.3 V. The light line shows the response for Pt/C($NaBH_4$) and the heavy line shows that obtained for Pt/C($scCO_2$). The initial potential was 0.0 V in each case.

passed during desorption of hydrogen from the platinum surface. Assuming the charge required to desorb a monolayer of hydrogen from platinum is 210 μC cm^{-2} [47], the ESA of the Pt/C($scCO_2$) and Pt/C(H_2O) electrocatalysts were 1.15 cm^2 and 1.0 cm^2, respectively. The higher ESA for the Pt/C($scCO_2$) is most likely due to its smaller average Pt particle size.

Rotating-disk electrode (RDE) voltammetry was used to assess the electrocatalytic efficiency of each electrocatalyst and compare their activities. Fig. 5 shows typical RDE voltammograms obtained at a range of rotation rates. In each case, the ORR onset potential was approximately 0.9 V. In acidic solution, the ORR can proceed by a 4-electron or a 2-electron route forming water or hydrogen peroxide, respectively. E^0 for the direct 4-electron route is 1.23 V, whereas E^0 for the 2-electron process is 0.695 V. Therefore, in the development of novel ORR electrocatalysts for fuel cells, the direct 4-electron route is preferable as higher cell voltages are obtained. Furthermore, the formation of hydrogen peroxide on noble metals can lead to homolysis of H_2O_2 generating hydroxyl radicals and Nafion, which is a commonly used electrolyte, is susceptible to attack by hydroxyl radicals [48]. Therefore, it is important to confirm that the direct $4e^-$ reduction route is operative. The Koutecky–Levich equation relates the limiting current density, i, to the rotation rate and can be used to calculate the number of electrons, n, transferred during the ORR:

$$\frac{1}{i} = \frac{1}{nFkC_O} + \frac{1}{0.62\,nFAD_O^{2/3}C_O\nu^{-1/6}\omega^{1/2}} \quad (1)$$

where F is the Faraday constant, C_O is the bulk concentration of O_2 dissolved in the electrolyte, k is the electron transfer rate constant, D_O is the diffusion coefficient of O_2, ν is the kinematic viscosity of the electrolyte (0.01 cm^2 s^{-1}) and ω is the rotation rate (rad s^{-1}). The insets of Fig. 5 show typical Koutecky–Levich plots obtained using each electrocatalyst, which were linear over the range of rotation rates studied. Using $D = 1.93 \times 10^{-5}$ cm^2 s^{-1} and $C = 1.13$ mM for O_2-saturated 0.5 M H_2SO_4 [49], n was calculated as 4.0 and 4.1 for Pt/C(H_2O) and Pt/C($scCO_2$), respectively from the slopes of the Koutecky–Levich plots. Therefore, these results demonstrate that the direct $4e^-$ reduction of O_2 to H_2O occurred predominantly at each Pt/C electrocatalyst.

3.4. Stability of Pt/C electrocatalysts

An enormous amount of work has been devoted to reducing the platinum loading within fuel cells, while retaining cell efficiency, and this has been achieved primarily by optimising the structure of the catalyst layers [50–53]. This effort can only be considered valuable if the microstructure within fuel cells remains relatively unchanged during operation. However, numerous studies have demonstrated that fuel cell operation can have a drastic effect on the structure of the catalyst layer. Pt dissolution and redeposition elsewhere within the fuel cell, as well migration and agglomeration of Pt nanoparticles can occur, causing a drop in power output [16–18]. In this study, we performed an accelerated stability test, in which the potential of the Pt/C-modified electrodes was electrochemically cycled in acid 5000 times between potential limits chosen to oxidise and reduce the Pt surface (0.6–1.1 V). The ESA and electrocatalytic activity of each catalyst was then compared before and after the stability test to investigate the effect of deposition route on electrocatalyst stability. Fig. 6 shows the CVs obtained at each Pt/C sample before and after potential cycling. In the case of Pt/C(H_2O), significant (23%) loss of ESA can be observed by the decrease in the charge passed during adsorption and desorption of hydrogen from the Pt surface (Fig. 6A). However, the CVs obtained at Pt/C($scCO_2$) show no detectable loss of ESA after potential cycling (Fig. 6B). The retention of ESA after potential cycling in the Pt/C($scCO_2$) sample is remarkable as numerous studies have shown rapid loss of electrochemical surface area when the potential of Pt/C electrodes was cycled to above 1 V [16,19,20,54].

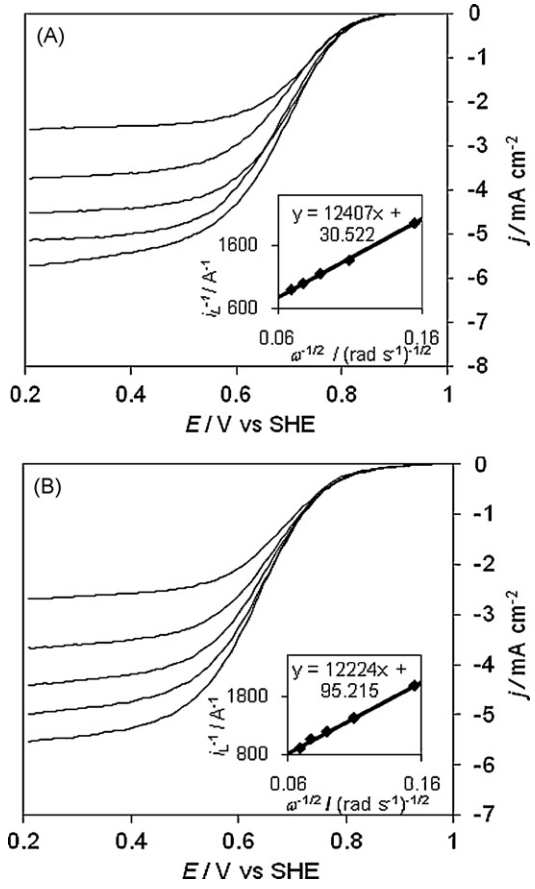

Fig. 5. ORR polarisation curves obtained at (A) Pt/C(H_2O) and (B) Pt/C($scCO_2$) at (from bottom to top) 2000, 1600, 1200, 800 and 400 rpm, respectively in O_2-saturated 0.5 M H_2SO_4. The voltammetric scan rate was 5 mV s^{-1} and the potential was scanned from 1.0 V to 0.2 V. The insets show Koutecky–Levich plots of i_L^{-1} vs $\omega^{-1/2}$ for each catalyst.

To investigate the effect of potential cycling on the electrocatalysts further, ORR polarisation curves were recorded before and after electrochemically cycling the electrocatalysts (Fig. 7). After cycling the potential between 1.1 V and 0.6 V 5000 times, the onset

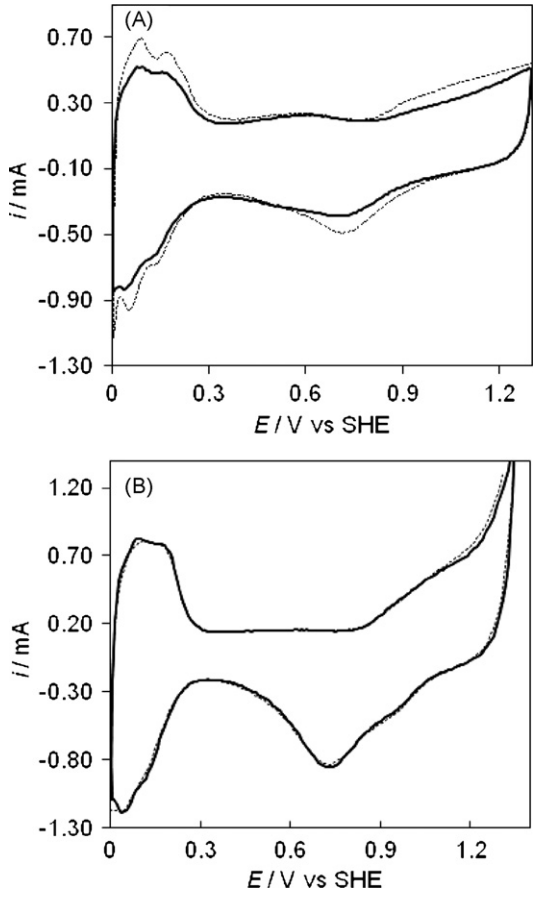

Fig. 6. CVs obtained at (A) Pt/C(H_2O) and (B) Pt/C($scCO_2$) in deoxygenated 0.5 M H_2SO_4 before (dashed line) and after (solid line) 5000 potential cycles between 0.6 V and 1.1 V at 0.5 V s^{-1} in 0.5 M H_2SO_4.

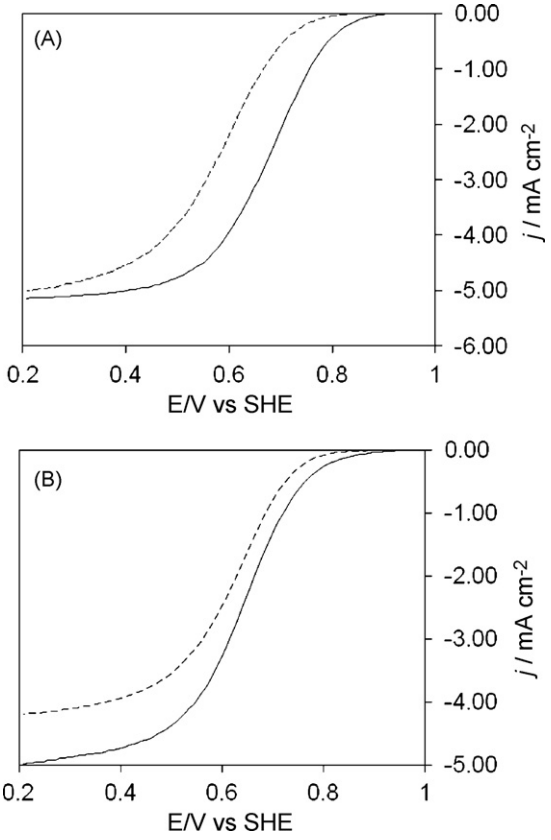

Fig. 7. Comparison of ORR polarisation curves obtained at (A) Pt/C(H_2O) and (B) Pt/C($scCO_2$) before (solid line) and after (dashed line) potential cycling from 1.1 V to 0.6 V 5000 times in 0.5 M H_2SO_4. The curves were recorded in O_2-saturated 0.5 M H_2SO_4 at a rotation rate of 1600 rpm, while the potential was swept from 1.0 V to 0.2 V at 5 mV s^{-1}.

potential for ORR at Pt/C($scCO_2$) shifted negative by approximately 30 mV. The current density, measured at 0.7 V (1600 rpm), dropped from 1.26 mA cm^{-2} to 0.75 mA cm^{-2}, a decrease of 40% (Fig. 7B). However, in the case of Pt/C(H_2O), the onset potential for the ORR at Pt/C(H_2O) shifted negative by approximately 85 mV. The current density, measured at 0.7 V (1600 rpm), dropped from 2.02 mA cm^{-2} to 0.53 mA cm^{-2}, a decrease of 74% (Fig. 7A). Therefore, these results clearly show that, while the Pt/C(H_2O) was slightly more active for the ORR than Pt/C($scCO_2$) prior to the stability test, Pt/C($scCO_2$) retained its electrocatalytic activity to a significantly larger extent.

TEM analysis was used to study the effect of potential cycling on the morphology of the Pt/C samples and correlate it with the loss of ESA and electrocatalytic activity. Fig. 8A shows a typical TEM image recorded for the Pt/C(H_2O) electrocatalyst after the accelerated stability test. Substantial growth of the Pt nanoparticles and a drastic increase in the particle size distribution upon potential cycling was observed, which is illustrated by comparing Fig. 8A with Fig. 1A. Large (10–30 nm) particles can be seen throughout the sample and the average particle size, estimated using TEM analysis after cycling, was 9.2 nm. This is more than twice the value estimated from TEM prior to electrochemical cycling (4.2 nm). Therefore, the loss of ESA and electrocatalytic activity by the Pt/C(H_2O) upon electrochemical cycling was due to the growth of the electrocatalyst particles. Fig. 8B shows a typical TEM image obtained for the Pt/C($scCO_2$) sample after potential cycling. In this case, the Pt nanoparticles remained reasonably well dispersed on the carbon and none of the large particles observed in the Pt/C(H_2O) sample were visible. The average size of the Pt nanoparticles in the Pt/C($scCO_2$) sample was 5.5 nm after potential cycling, which is significantly smaller than that estimated for the Pt/C(H_2O) sample and still close to the optimum size for electrocatalysis (1–5 nm). In addition, the particle size distribution remained reasonably small after potential cycling. Therefore, it appears that the increased retention of ESA and electrocatalytic activity by the Pt/C($scCO_2$) compared to the Pt/C(H_2O) is due to the fact that, even though the average particle size increased slightly, the Pt particles remained reasonably small and well dispersed on the carbon during the accelerated stability test. As described previously, the loss of ESA and electrocatalytic activity from Pt/C electrocatalysts can occur by dissolution and redeposition of Pt, and by migration and coalescence of the Pt nanoparticles [18]. If significant Pt dissolution and redeposition had occurred in this study, we would expect a distribution of reasonably spherical, uniformly sized nanoparticles to be produced after electrochemically cycling the electrocatalysts [18]. However, as shown in Fig. 8A, an array of irregularly shaped Pt particles, with a wide range of particle sizes was produced upon potential cycling. Therefore, it appears that the loss of ESA occurred primarily by migration (surface diffusion) and coalescence of the Pt nanoparticles and that the Pt particles formed in the supercritical fluid are more resistant to migration and agglomeration. While it is known that larger Pt particles are less susceptible to particle coalescence during potential cycling [55], previous studies have also shown that Pt particles that are highly dispersed on carbon black are more resistant to agglomeration than those that are less well dispersed [56,57]. As shown in Fig. 1, the particles in the Pt/C($scCO_2$) sample appeared to be slightly more highly dispersed across the carbon support compared to the particles in Pt/C(H_2O) and this may be due to the unique solvent properties of the supercritical fluid. Therefore, it is possible that the apparent resistance to agglomeration and electrochemi-

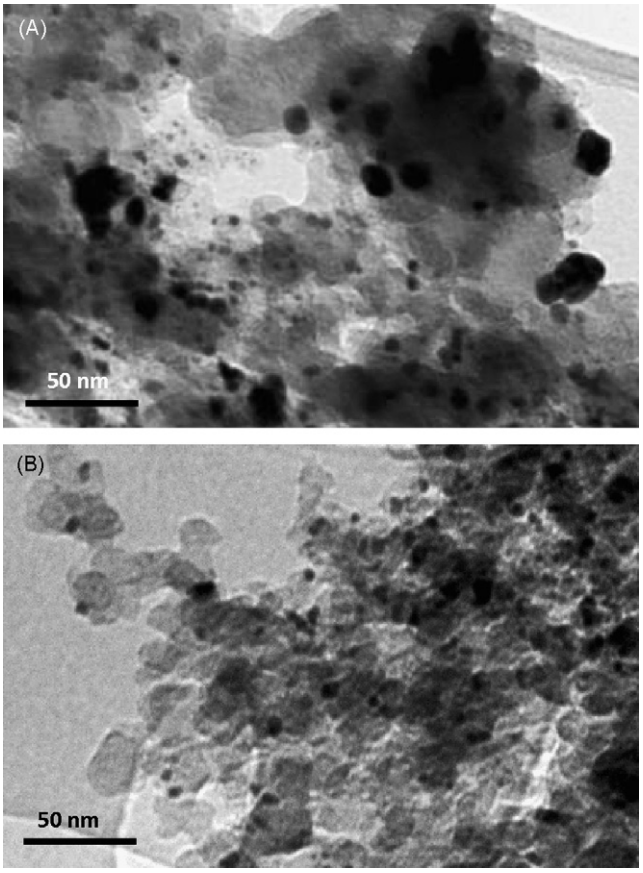

Fig. 8. TEM images of (A) Pt/C(H_2O) and (B) Pt/C($scCO_2$) after 5000 cycles between 0.6 V and 1.1 V at a scan rate of 0.5 V s^{-1} in 0.5 M H_2SO_4.

cal stability of the catalyst formed in $scCO_2$ are due to the high dispersion achieved using this method. However, we cannot fully discount the effect of the impregnation medium on the carbon support and the support–particle interactions. Further work is required to fully establish the mechanism of stabilisation of the electrocatalysts formed using $scCO_2$. Nonetheless, it is clear that supercritical fluid impregnation is promising for the fabrication of more stable fuel cell cathodes.

4. Conclusions

Pt/C catalysts for oxygen reduction were synthesised using supercritical fluid impregnation and a wet chemical method and their durability was examined using an accelerated stability test, in which the electrocatalysts were subjected to repeated potential cycling in acid. During the stability test, the Pt/C formed in supercritical CO_2 lost a negligible amount of electrochemical surface area whereas the Pt/C formed in H_2O lost a significant proportion of its electrochemical surface area. Significant agglomeration of the Pt particles in the Pt/C(H_2O) was also observed while the Pt particles within the Pt/C($scCO_2$) remained reasonably well dispersed on the carbon support. Electrocatalytic measurements performed before and after testing showed that the Pt/C($scCO_2$) lost significantly less electrocatalytic activity than the Pt/C(H_2O). Further work is required to fully establish the mechanism of stabilisation of these catalysts but it may be due to the high catalyst particle dispersion achievable using supercritical fluid impregnation. Furthermore, it will be very interesting to compare the stability of the catalyst formed using supercritical fluid impregnation with catalysts formed using alternative synthetic routes and this will be addressed in a future contribution. In conclusion, these results show that supercritical fluid impregnation of carbon using organometallic precursors and thermal reduction in an inert atmosphere is not only a very clean method for electrocatalyst synthesis, it is very promising for the fabrication of more durable Pt cathode electrocatalysts for fuel cells.

Acknowledgements

We thank the UK EPSRC for funding this work through the DICE (Driving Innovation in Chemistry and Chemical Engineering) Project under the Science and Innovation Award (Grant Number EP/D501229/1). We also thank the Nottingham Nanotechnology and Nanoscience Centre for access to electron microscopy facilities.

References

[1] H. Yano, M. Kataoka, H. Yamashita, H. Uchida, M. Watanabe, Langmuir 23 (2007) 6438.
[2] V. Stamenković, T.J. Schmidt, P.N. Ross, N.M. Marković, J. Phys. Chem. B 106 (2002) 11970.
[3] M. Wakisaka, H. Suzuki, S. Mitsui, H. Uchida, M. Watanabe, J. Phys. Chem. C 112 (2008) 2750.
[4] H. Chang, S.–H. Joo, C. Pak, J. Mater. Chem. 17 (2007) 3078.
[5] B. Fang, J.H. Kim, M. Kim, J.-S. Yu, Chem. Mater. 21 (2009) 789.
[6] O. Savadogo, K. Lees, K. Oishis, S. Mitsushimaa, N. Kamiyaa, K.-I. Otaa, Electrochem. Commun. 6 (2004) 105.
[7] M.-H. Shao, K. Sasaki, R.R. Adzic, J. Am. Chem. Soc. 128 (2006) 3526.
[8] J.L. Fernández, V. Raghuveer, A. Manthiram, A.J. Bard, J. Am. Chem. Soc. 127 (2005) 13100.
[9] M. Sanles-Sobrido, M.A. Correa-Duarte, S. Carregal-Romero, B. Rodríguez-González, R.A. Álvarez-Puebla, P. Hervés, L.M. Liz-Marzán, Chem. Mater. 21 (2009) 1531.
[10] B. Seger, P.V. Kamat, J. Phys. Chem. C 113 (2009) 7990.
[11] C.L. Sun, L.C. Chen, M.C. Su, L.S. Hong, O. Chyan, C.-Y. Hsu, K.H. Chen, T.F. Chang, L. Chang, Chem. Mater. 17 (2005) 3749.
[12] J. Shim, K.Y. Joung, J.H. Ahn, W.M. Lee, J. Electrochem. Soc. 154 (2007) B165.
[13] C. Roychowdhury, F. Matsumoto, P.F. Mutolo, H.D. Abruña, F.J. DiSalvo, Chem. Mater. 17 (2005) 5871.
[14] H. Li, G. Sun, Y. Gao, Q. Jiang, Z. Jia, Q. Xin, J. Phys. Chem. C 111 (2007) 15192.
[15] R. Borup, J. Meyers, B. Pivovar, Y.S. Kim, R. Mukundan, N. Garland, D. Myers, M. Wilson, F. Garzon, D. Wood, P. Zelenay, P. More, K. Stroh, T. Zawodzinski, J. Boncella, J.E. McGrath, M. Inaba, K. Miyatake, M. Hori, K. Ota, Z. Ogumi, S. Miyata, A. Nishikata, S. Siroma, Y. Uchimoto, K. Yasuda, K.-I. Kimijimaand, N. Iwashita, Chem. Rev. 107 (2007) 3904.
[16] K. Yasuda, A. Taniguchi, T. Akita, T. Oiroi, Z. Siroma, Phys. Chem. Chem. Phys. 8 (2006) 746.
[17] Y. Shao-Horn, W.C. Sheng, S. Chen, P.J. Ferreira, E.F. Holby, D. Morgan, Top. Catal. 46 (2007) 285.
[18] Y. Shao, R. Kou, J. Wang, V.V. Viswanathan, J.H. Kwak, J. Liu, Y. Wang, Y. Lin, J. Power Sources 185 (2008) 280.
[19] P.J. Ferreira, G.J. la O', Y. Shao-Horn, D. Morgan, R. Makharia, S. Kocha, H.A. Gasteiger, J. Electrochem. Soc. 152 (2005) A2256.
[20] R.L. Borup, J.R. Davey, F.H. Garzon, D.L. Wood, M.A. Inbody, J. Power Sources 163 (2006) 76.
[21] B. Lim, M. Jiang, P.H.C. Camargo, E.C. Cho, J. Tao, X. Liu, Y. Zhu, Y. Xia, Science 324 (2009) 1302.
[22] J. Zhang, K. Sasaki, E. Sutter, R.R. Adzic, Science 315 (2007) 220.
[23] X. Li, S. Park, B.N. Popov, J. Power Sources 195 (2010) 445.
[24] H. Wakayama, Y. Fukushima, Ind. Eng. Chem. Res. 45 (2006) 3328.
[25] C.A. Johnson, S. Sharma, B. Subramaniam, A.S. Borovik, J. Am. Chem. Soc. 127 (2005) 9698.
[26] S. Moisan, V. Martinez, P. Weisbecker, F. Cansell, S. Mecking, C. Aymonier, J. Am. Chem. Soc. 129 (2007) 10602.
[27] A. Cooper, in: M.F. Kemmere, T. Meyer (Eds.), Supercritical Carbon Dioxide in Polymer Reaction Engineering, Wiley, 2005 (Chapter 11).
[28] M.C. McLeod, W.F. Gale, C.B. Roberts, Langmuir 20 (2004) 7078.
[29] M. Ji, X. Chen, C.M. Wai, J.L. Fulton, J. Am. Chem. Soc. 121 (1999) 2631.
[30] Y. Lin, X. Cui, C. Yen, C.M. Wai, J. Phys. Chem. B 109 (2005) 14410.
[31] Y. Zhang, C. Erkey, Ind. Eng. Chem. Res. 44 (2005) 5312.
[32] R. Jiang, Y. Zhang, S. Swier, X. Wei, C. Erkey, H.R. Kunz, J.M. Fenton, Electrochem. Solid State Lett. 8 (2005) A611.
[33] A. Bayrakçeken, A. Smirnova, U. Kitkamthorn, M. Aindow, L. Türker, I. Eroğlu, C. Erkey, J. Power Sources 179 (2008) 532.
[34] C.H. Yen, K. Shimizu, Y.-Y. Lin, F. Bailey, I.F. Cheng, C.M. Wai, Energy Fuels 21 (2007) 2268.
[35] Y. Lin, X. Cui, C.H. Yen, C.M. Wai, Langmuir 21 (2005) 11474.
[36] A. Bayrakcekena, U. Kitkamthornb, M. Aindowb, C. Erkey, Scripta Mater. 56 (2007) 101.
[37] Y. Zhang, C. Erkey, J. Supercrit. Fluids 38 (2006) 252.
[38] J. Zhang (Ed.), PEM Fuel Cell Electrocatalysts and Catalyst Layers: Fundamentals and Applications, Springer-Verlag, London, 2008.

[39] K. Kinoshita, J. Electrochem. Soc. 137 (1990) 845.
[40] S. Mukerjee, J. McBreen, J. Electroanal. Chem. 448 (1998) 163.
[41] J. Perez, E.R. Gonzalez, E.A. Ticianelli, Electrochim. Acta 44 (1998) 1329.
[42] O. Antoine, Y. Bultel, R. Durand, J. Electroanal. Chem. 499 (2001) 85.
[43] K.J.J. Mayrhofer, B. Blizanac, M. Arenz, V.R. Stamenkovic, P.N. Ross, N.M. Markovic, J. Phys. Chem. B 109 (2005) 14433.
[44] H. Bönnemann, K.S. Nagabhushana, R.M. Richards, in: D. Astruc (Ed.), Nanoparticles and Catalysis, Wiley–VCH, 2007, p. 77.
[45] B. Cangül, L.C. Zhang, M. Aindow, C. Erkey, J. Supercrit. Fluids 50 (2009) 82.
[46] Rodrigo Fernández-Pacheco, Manuel Arruebo, ClaraMarquina, Ricardo Ibarra, Jordi Arbiol, Jesús Santamaría, Nanotechnology 17 (2006) 1188.
[47] A.J. Bard, L.R. Faulkner, Electrochemical Methods: Fundamentals and Applications, 2nd edn., Wiley, New York, 2001.
[48] V.A. Sethuraman, J.W. Weidner, A.T. Haug, S. Motupally, L.V. Protsailo, J. Electrochem. Soc. 155 (2008) B50.
[49] M.S. El-Deab, T. Ohsaka, Electrochim. Acta 47 (2002) 4255.
[50] J.F. Whitacre, R.D. Murphy, A. Marrie, S.M. Yalisove, Electrochem. Commun. 11 (2009) 655.
[51] P. Ramesh, M.E. Itkis, J.M. Tang, R.C. Haddon, J. Phys. Chem. C 112 (2008) 9089.
[52] J.M. Tang, K. Jensen, M. Waje, W. Li, P. Larsen, K. Pauley, Z. Chen, P. Ramesh, M.E. Itkis, Y. Yan, R.C. Haddon, J. Phys. Chem. C 111 (2007) 17901.
[53] J.M. Song, S. Suzuki, H. Uchida, M. Watanabe, Langmuir 22 (2006) 6422.
[54] B. Merzougui, S. Swarthirajan, J. Electrochem. Soc. 153 (2006) A2220.
[55] Y. Shao, G. Yin, Y. Gao, J. Power Sources 171 (2007) 558.
[56] A. Honji, T. Mori, K. Tamura, Y. Hishinuma, J. Electrochem. Soc. 135 (1988) 355.
[57] A. Honji, T. Mori, Y. Hishinuma, J. Electrochem. Soc. 137 (1990) 2084.